Design and Evaluation of a Mobile Ankle Exoskeleton With Switchable Actuation Configurations

Jianyu Chen, Jianda Han, and Juanjuan Zhang

***Abstract*—Lower limb exoskeletons with proper assistance can improve the mobility of people with leg impairments. Prior studies have shown that tethered ankle exoskeletons can reduce the metabolic cost during walking and running, but few mobile ankle exoskeletons can achieve similar performance. The additional weight of the actuation system and compromised control performance decrease the assistance efficiency. Here, we developed a mobile exoskeleton that can provide plantarflexion torque assistance at the ankle. The actuation system is switchable between a single- and dual-motor ones to adapt to different users and tasks. The single-motor system can achieve lighter weight and better transparency while the dual-motor one can provide higher assistance. The single-motor exoskeleton system has a 0.95 kg weight worn on the leg with another 1.15 kg power belt mounted on the waist. The dual-motor system can provide up to 100 N·m assistive torque and reduce an average of 32.5% of soleus muscle activity in preliminary tests. A real-time controller was implemented in an integrated embedded system and achieved high torque control performance. The closed-loop bandwidths of the single- and the dual-motor systems were 13.0 and 15.3 Hz, respectively. The average root-mean-squared torque tracking error was 2.6% of peak torque during walking and running. The mobile ankle exoskeleton can assist for 3 h of continuous active walking or running with an integrated 4500 mAh battery, making it promising in investigating assistance strategies off the treadmill.**

***Index Terms*—Mobile ankle exoskeleton, switchable actuation configuration, torque control, wearable robotics.**

Manuscript received November 22, 2021; revised March 26, 2022; accepted April 20, 2022. Recommended by Technical Editor M. Tavakoli and Senior Editor X. Chen. This work was supported by the National Natural Science Foundation of China under Grant 62073179. *(Corresponding author: Juanjuan Zhang.)*

The authors are with the Tianjin Key Laboratory of Intelligent Robotics, Institute of Robotics and Automatic Information Systems, Nankai University, Tianjin 300350, China (e-mail: jychen@mail.nankai.edu.cn; hanjianda@nankai.edu.cn; juanjuanzhang@nankai.edu.cn).

This work involved human subjects or animals in its research. Approval of all ethical and experimental procedures and protocols was granted by the Ethical Committee of Nankai University.

Color versions of one or more figures in this article are available at https://doi.org/10.1109/TMECH.2022.3175731.

Digital Object Identifier 10.1109/TMECH.2022.3175731

I. Introduction

In THE past decades, researchers have designed various exoskeletons to improve locomotion performance [1], [2], carry load [3], [4], and aid in rehabilitation [5], [6]. However, by group optimization through evolution and individual learning during maturation, human natural locomotion is highly efficient and is difficult to assist. The additional weight of exoskeletons and restrictions in unassisted directions disturb the natural dynamics of human movements, thereby incur metabolic penalty and fatigue [7]. In addition, the interpersonal differences make the optimal assistance strategy difficult to identify, and improper assistance will further disturb human locomotion and increase energy consumption [8], [9].

In order to investigate assistance strategies and explore the possibility of enhancing locomotor performance, many tethered exoskeleton systems have been developed with lightweight end effectors and off-board actuators [10]–[12]. Utilizing powerful and versatile motors, tethered exoskeletons can provide a wide range of assistances with high tracking performance. Human-in-the-loop optimization further helps these exoskeletons find optimal assistance parameters and be more effective in reducing metabolic costs [1], [13]. However, with the connection of tether, the locomotion of human–exoskeleton systems are restricted on treadmills, leaving the assistance of overground gaits on different terrains less explored.

Currently, the performances of most mobile exoskeletons are still unsatisfactory. The reported optimal exoskeleton assistance torque can be higher than 0.8 $\mathrm{N{\cdot}m{\cdot}kg^{-1}}$ at the ankle [1], while few mobile devices can achieve so [4], [14], [15]. The gap between mobile and tethered exoskeletons mainly comes from the limited actuator power density of the former. The additional weight of the motors aggravates metabolic penalty during locomotion. Designers have to balance the system weight and actuation power, making it difficult to adapt to the requirements of different users and applications.

In this article, to address the challenge of balancing system weight and actuator power and improving the capacity of mobile exoskeletons, we utilized modularized actuators with parallel connections to construct a switchable actuation system. The contributions of this study are as follows:

1) We developed a versatile, mobile ankle exoskeleton platform with a lightweight end effector, switchable actuation

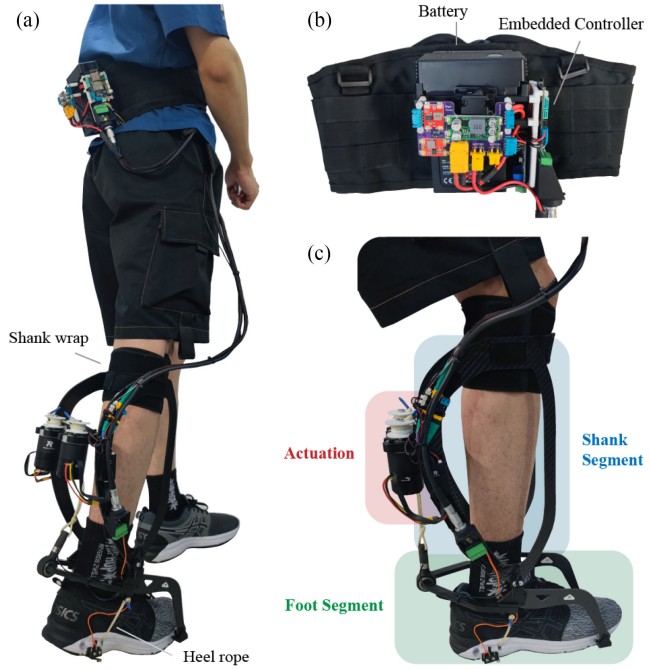

Fig. 1. (a) Overview of a mobile, lightweight ankle exoskeleton with dual-motor actuation configuration. The total mass of the exoskeleton with two motors is 2.55 kg with (b) a 1.15 kg power belt mounted on the waist and (c) 1.4 kg end effector and actuation system worn on the leg.

Fig. 2. Exploded view of the exoskeleton end effector. By utilization of carbon fibers and aluminum alloy, the end effector was 0.5 kg without actuator.

configurations, and a high-accuracy embedded torque tracking controller.

2) We designed and optimized the structure of the end effector with topology optimization, making it lightweight, high strength, and compliant to wear.
3) This is the first mobile ankle exoskeleton utilizing parallel connection of modularized actuators to achieve high assistance. This method can easily be extended to handle more motors to achieve higher assistance capacity.
4) The torque tracking performance of our system with the proposed embedded torque controller is better than the existing mobile ankle exoskeletons.
5) Preliminary transparency tests and physiological experiments were conducted and demonstrated the effectiveness of our systems. The single-motor system, which showed better transparency, is helpful in improving the mobility of patients and the elderly. The dual-motor system with high torque capability is promising in investigating off-treadmill assistance strategies and providing effective assistance in strenuous physical activities.

II. Materials and Methods

The exoskeleton comprises an end effector with an optimized lightweight structure, an integrated switchable actuation system, and a power waist belt (see Fig. 1). By geometry optimization, the structure of the exoskeleton end effector can provide fairly high assistance with compliance. The actuation system was designed with modularization, which can switch between a single- and a dual-motor configurations. An embedded system was developed to measure sensor signals, process data, implement control algorithms, and communicate with the host PC. An admittance controller with compensation loops was implemented and provided high-accuracy torque tracking performance. The total mass of the mobile exoskeleton with a single-motor configuration is 2.1 kg, with 0.95 kg distal mass worn on the leg. The exoskeleton with the dual-motor actuation is 0.45 kg heavier but can provide 100 N·m assistive torque and, thus, more assistance benefits.

A. Ankle Exoskeleton End Effector

The ankle exoskeleton end effector is composed of the shank, foot, and toe segments, which are connected by rotational joints (see Fig. 2). It was redesigned and optimized from a previous prototype [12]. The shank segments are attached below the knee via a padded strap. A high-tensile rope tied on the foot segment interfaces with the human heel to apply for powerful assistance. By the utilization of carbon fiber and aluminum alloy, the total mass of an end effector was reduced to 0.5 kg, making it compliant and comfortable to wear.

The geometry of the carbon fiber strut was designed to be spindle shaped (see Fig. 2) to reduce the possible contact between the human leg and exoskeleton structure. The hollowed-out shape also eases the installation of electromyography (EMG) sensors and optical markers. An aluminum crossbar connects the two shank struts and provides frontal plane structural supports. A groove along the crossbar makes it convenient to connect with components, such as the switchable actuation system (see Fig. 3). It can also be connected to an off-board motor through Bowden cables, translating the end effector into a tethered ankle

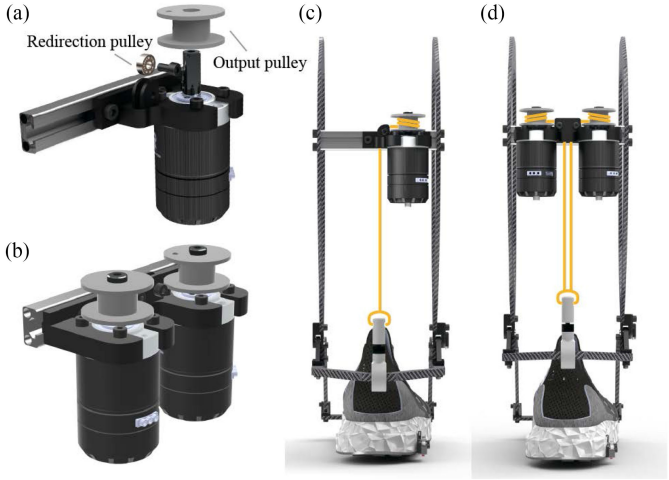

Fig. 3. Actuation system was designed with switchable configurations, which can alter between single- (a), (c) and dual-motor ones (b), (d) for different users and tasks. A high-strength cable redirected by the pulley connects the load cell and the output pulley of motor.

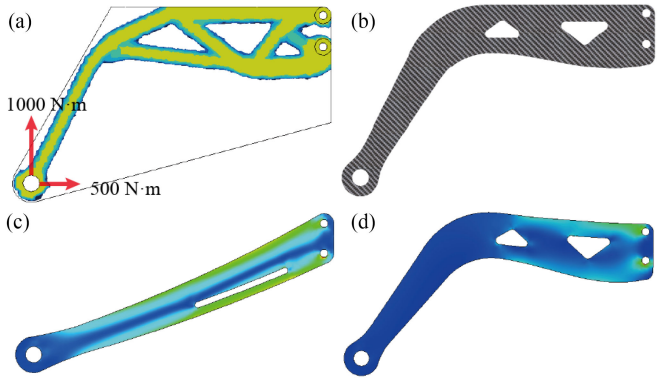

Fig. 4. (a) Topology optimization of foot strut from a selected initial shape, which is shown as the black lines. External force was applied on the metatarsophalangeal joint as the red row. The geometry of the foot strut (b) was designed based on topology optimization result. FEA were conducted on (c) our previous design and (d) the optimized design with the same force settings.

exoskeleton system for investigating assistance strategies on the treadmill.

Two ankle joint assemblies connect the shank segment and the foot segment using two ball bearings on each side. One end of the axle was cut as a D shape to be fixed with the lower joint strut in assembly so that a magnetic encoder installed on it can instrument the ankle joint angle. Joint rotation range was restricted by the shape of lower and upper joint structs in assemblies, allowing for 50° plantarflexion to 30° dorsiflexion and providing a hard stop.

The foot segment comprises two foot struts and a heel bracket. The heel bracket is mounted behind the ankle joint assemblies to provide a long lever arm. Made out of carbon fiber, this component provides series elasticity with an equivalent stiffness of 217 N·m·rad^{-1}. A load cell was fixed at the back side of the heel bracket by the selected laser sintering (SLS) nylon seat to sense the assistive torque. Two SLS nylon pads were glued on the back side of the carbon fiber to form a circular shaft for the load cell seat to rotate, ensuring the measurement direction of the load cell collinear with the applied force.

The foot struts need to have high strength for directly interacting with the ground. We used topology optimization to determine an appropriate shape of foot carbon fiber. The optimization was conducted by applying 1000 N vertical force and 500 N horizontal force to the toe joint (see Fig. 4) to simulate the ground reaction force during locomotion. Two mounting holes at the ending of carbon fiber were set as fixed. The topology optimization started from an initial quadrilateral shape (black-contoured shaped in Fig. 4(a), which is defined by the allowed area) and aimed to reduce 80% of the initial material mass. The remained boomerang area after topology optimization indicates the most effective structural element under the applied force, so the final shape of the struct was designed, as shown in Fig. 4(b). We further evaluated the optimized design by finite element analysis (FEA) to the same force settings in topology optimization. Compared with the previous design [see Fig. 4(c)], the new design [see Fig. 4(d)] has a significantly reduced stress concentration, and the maximum displacement was reduced from 1.6 to 0.52 mm under the applied force.

B. Actuation System

The actuation system was designed with modularization to be switchable between a single- and dual-motor configurations. It can easily be extended to handle more motors for applications requiring higher assistance. Each motor module weighs 0.45 kg. Transmitted by a cable, each module can provide 50 N·m max torque to an ankle and generate maximum 200 W mechanical power.

The actuators pull the back side of the foot bracket by unidirectional cables (see Fig. 3). Similar to the tethered exoskeleton systems [12], the unidirectional cable can isolate the human joint from motor damping, providing low impedance when slacked, which is useful in zero-torque mode. The cable also separates the actuators from each other, which means that each actuator can generate assistive torque separately without the need for complete synchronization in angular position. Motors are mounted on an aluminum motor seat and connected to the shank crossbar. Their shafts were installed to be parallel to the shank to get a compact construction. For each motor module, a high-strength cable redirected by a pulley [see Fig. 3(a) and (b)] connects the output pulley of the motor to the load cell assembly [see Fig. 3(c) and (d)]. The motor output pulley radius and the device's ankle lever arm are 10 and 125 mm.

C. Sensing and Electrical Hardware

The mobile exoskeleton system senses human–robot interactions by several sensors [see Fig. 5(a)]. An absolute magnetic encoder (PQY18, ACCNT, China) is fixed on the ankle joint assembly with a magnet glued into the ankle axle. A load cell (DYMH-106, DAYSENSOR, China) is seated at the narrow side of the heel bracket, measuring the cable force. The assistance torque is calculated by multiplying the measured force and lever arm. Heel strike detected by a switch (KW12, Risym, China) is

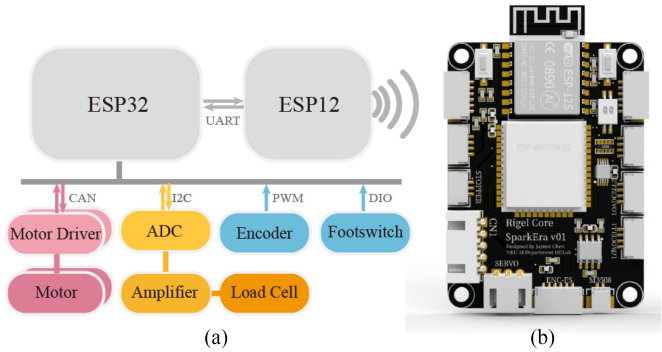

Fig. 5. (a) Exploded views of integrated sensors. (b) Maximum torque and bandwidth tests setup. The exoskeleton was settled on an aluminum frame with the foot segment locked by a carbon fiber struct.

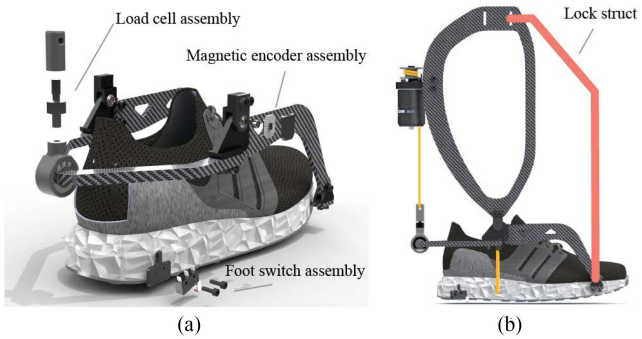

Fig. 6. (a) Flow diagram and (b) overview of the integrated embedded system.

used to signal the start of a gait cycle. The switch is attached on the outer side surface of the shoe through an SLS nylon pad. Each brushless dc geared motor (M3508, DJI, China) was driven by a motor driver (C620, DJI, China).

An embedded system (see Fig. 6) was developed for measuring signal, processing data, and implementing control algorithm. A 32-bit microcontroller unit (MCU) ESP32 (ESP32-WROOM-32D, Espressif, China) was used to execute the control algorithm with another MCU ESP12 communicating with the host PC. The ESP32 communicates with motor drivers by controller area network communication protocol to get motor state signals and send control commands. The signal from load cell is amplified by an amplifier (DY510, DAYSENSOR, China), and the MCU acquires the analog signal through ADC. The absolute magnetic encoder sends a pulsewidth modulation signal to MCU, informing the absolute ankle joint angle. The ESP32 performs high-level and low-level control computations at 1000 Hz. The measured signals and operating state are sent to ESP12 by Universal Asynchronous Receiver/Transmitter and then delivered to a telemetry laptop through the wireless network for real-time data visualization and recording at 200 Hz. The whole system is powered by a 4500 mAh battery (TB47S, DJI, China).

D. Control Approach

A hierarchical control approach was developed for this cable-driven exoskeleton. The controller switches between torque and position control on the change of gait phase. During the stance phase, the high-level controller generates an assistive torque profile, and the low-level controller drives the motor to track the desired torque. During the swing phase, the controller switches into position control mode, following the individual's active movements. An admittance controller with motion and current compensations was implemented [see Fig. 7(a)]. The high-level controller generates the desired assistive torque τ_d. The applied torque τ_a and ankle velocity $\dot{\theta}_a$ are measured from a human–exoskeleton system by load cell and encoder, respectively. The admittance controller transforms a torque error e_τ into a desired motor velocity $\dot{\theta}_d$ by a virtual admittance equation

$$\frac{\dot{\theta}_d}{e_\tau} = \frac{1}{M_v s + D_v} \tag{1}$$

where M_v and D_v define the virtual inertia and virtual damping. The virtual inertia determines how fast the motor responds to the tracking error. The virtual damping helps reduce the shock of motor velocity, thus improves the compliance between the actuator and the human–exoskeleton system. The desired motor velocity is then tracked by the inner motor velocity control loop using a proportional–integral–derivative controller and generates current commands to the motor drive. Due to the nonlinearity of exoskeleton and the disturbances from the ankle motions, the general admittance controller does not show decent tracking performance. To further improve tracking accuracy, motion and current compensation loops were implemented

$$\dot{\theta}_f = K_f^v \cdot R \cdot \dot{\theta}_a,\ I_f = K_f^I \cdot \frac{\tau_d}{R} \tag{2}$$

where K_f^v and K_f^I represent the motion and current compensation gain, and R is the effective aspect ratio between motor output pulley radius and exoskeleton joint lever arm. Aided by compensation loops, the feedback admittance controller only needs to eliminate the errors caused by unmodeled dynamics and nonlinearity, making it more stable and effective.

During the swing phase, the position controller [see Fig. 7(b)] follows the wearer's active ankle movements:

$$\theta_d = R \cdot \theta_a - \theta_0 \tag{3}$$

where θ_d is the desired motor angle, θ_a is ankle joint angle, and θ_0 is a slack margin. The slack margin helps unidirectional cables keep slacked during position control. The motion compensation and current compensation were also employed, aiming to remove any possible cable force

$$\dot{\theta}_f = K_f^v \cdot R \cdot \dot{\theta}_a,\ I_f = -K_f^I \cdot \frac{\tau_a}{R}. \tag{4}$$

For a dual-motor system, each motor is controlled by an independent lower level controller, while the gait state machine and high lever controller were shared to generate the same desired torque or position trajectories. The parameters in the controller were tuned in pilot tests and listed in Table I.

III. Experiment and Results

We conducted a series of experiments to evaluate the performance of the mobile exoskeleton. The maximum torque

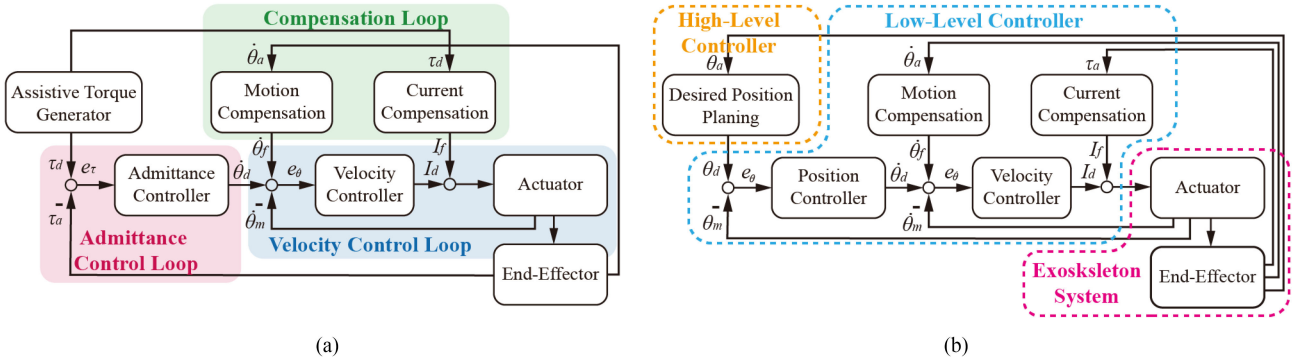

Fig. 7. Schematics of (a) torque and (b) position controller. The controller switches between torque and position control on the change of gait phases.

TABLE I
LOW-LEVEL TORQUE CONTROL PARAMETER VALUES

Parameter	M_v	D_v	K_f^v	K_f^I	R	θ_0
Value	2.5	0.2	0.5	0.15	0.125	20

and bandwidth of each actuation configuration were measured by closed-loop step response and frequency response tests, respectively. Participant-involved experiments were performed to evaluate the exoskeleton's transparency, torque tracking performance, and physiology effectiveness. All participants were provided with written informed consent before completing the experiments, which was approved by the ethical committee of Nankai University.

A. Transparency Tests

We conducted the preliminary mechanical transparency experiments on a single healthy participant (1.70 m, 72 kg, 24 years) to test the influence on human locomotion of the mobile ankle exoskeleton when unpowered under both actuation configurations. The participant was asked to walk on a treadmill at 1.25 m·s^{-1} in three conditions: normal walking (NW) condition without wearing the exoskeleton (NW), zero-torque condition with single-motor actuation (S-ZT), and zero-torque condition with dual-motor actuation (D-ZT). During zero-torque conditions, the exoskeleton was unpowered with the driving cables slacked. The subject's kinematic and ground reaction force signals were measured to calculate the joint moments. Kinematic data were recorded by nine motion capture cameras (Oqus 700, Qualisys, Sweden), and ground reaction force was measured by a treadmill (Bertec, USA). The joint angles and moments were computed using inverse kinematics tool and inverse dynamics tool of OpenSim [16].

Fig. 8 shows the subject's kinematic and dynamic responses under different conditions. The maximum ankle dorsiflexion angle decreased 6.4° under single-motor actuation and 9.1° under dual-motor actuation, compared with NW. Maximum ankle plantarflexion moment increased 1.9% under single-motor actuation and 3.6% under dual-motor actuation. Maximum hip flexion moment increased 5.4% under single-motor actuation and 10.5% under dual-motor actuation.

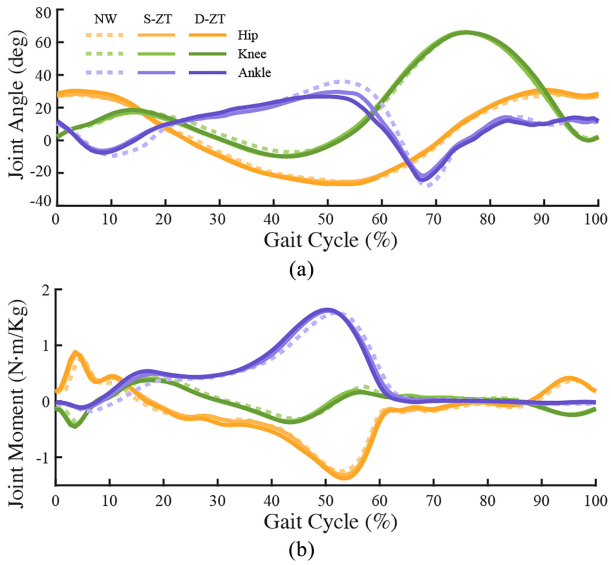

Fig. 8. Exoskeleton transparency tests under two different actuation configurations when applied zero torque compared with NW.

B. Maximum Torque Step Response Tests

We implemented the torque step response tests to evaluate the maximum torque assistance capability under two different actuation configurations. For the purpose of safety, the exoskeleton was fixed on an aluminum frame with the foot segments and the shank segments locked together by two carbon fiber structs on each side [see Fig. 5(b)]. Desired torques were generated as a step signal rising at 0.2 s and held for more than 0.8 s. The torque magnitudes were 50 and 100 N·m for single motor and dual motor, respectively. Each test was performed ten times, and the results were averaged (see Fig. 9). The rise time were 57 ms for single-motor configuration and 81 ms for dual-motor configuration.

C. Closed-Loop Torque Bandwidth Tests

We performed closed-loop torque bandwidth tests under two different actuation configurations to test the torque tracking performance in static condition. The exoskeleton structure was fixed with the same way described previously. The desired

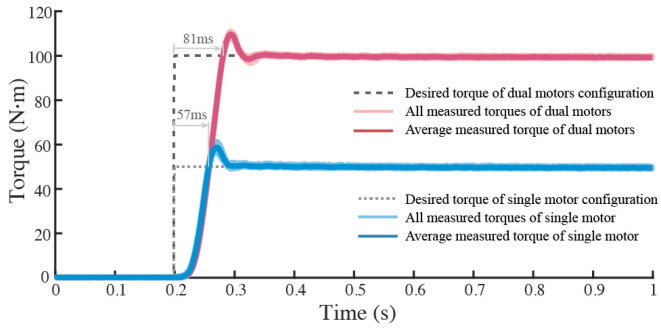

Fig. 9. Maximum torque tests for single- and dual-motor configurations.

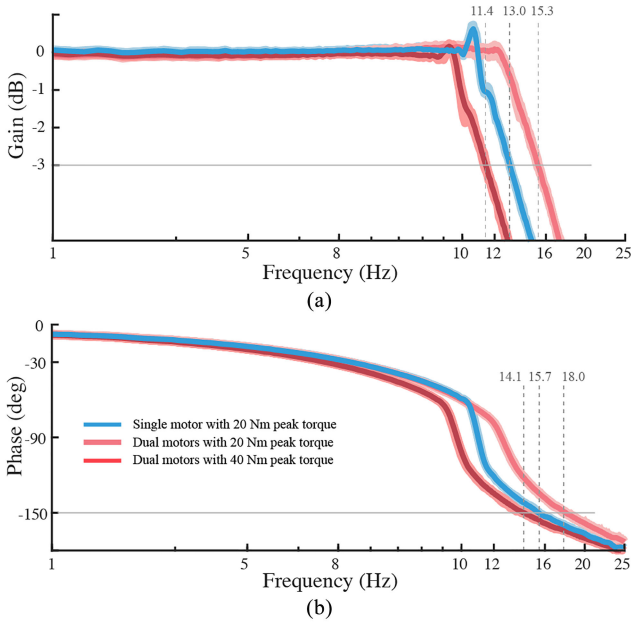

Fig. 10. Torque frequency response of the mobile exoskeleton with different actuation configurations at different levels of peak torque in the closed-loop bandwidth tests. The lines with light color depict results in each experiment, and the lines with dark color represent the averaged result.

torques were generated as linear chirps with the frequency continuously changing from 1 to 25 Hz. Their magnitude were set at 20 N·m for single motor and dual motor. Another 40 N·m magnitude desired torque test was conducted only on dual-motor configuration. Every condition was performed ten times and the results were averaged.

Bode plots (see Fig. 10) were generated by the desired and measured torque signals using fast Fourier transform. Bandwidth was calculated as the decline of the -3 dB cut-off frequency and the 30° phase margin. The gain-limited closed-loop bandwidths for single motor and dual motor under 20 N·m magnitude were 13.0 and 15.3 Hz, respectively. The phase-limited closed-loop bandwidths were 15.7 and 18.0 Hz. The gain-limited and phase-limited bandwidths for dual motor under 40 N·m peak torque were 11.4 and 14.1 Hz, respectively.

TABLE II
TORQUE PROFILE AND RMS-E FOR 12 ASSISTANCE CONDITIONS

	Conditions				Results	
	T_r (%)	T_f (%)	T_p (%)	Γ_p (N·m)	RMS-E (N·m)	RMS-E (%)
SW1	20	12	45	30	0.52	1.7
SW2	23	10	48	30	0.54	1.8
SW3	25	8	50	30	0.56	1.9
SR1	10	15	20	30	0.96	3.2
SR2	12	12	22.5	30	1.07	3.6
SR3	15	10	25	30	0.87	2.9
DW1	20	12	45	60	1.07	1.8
DW2	23	10	48	60	0.80	1.3
DW3	25	8	50	60	0.98	1.6
DR1	10	15	20	50	2.20	4.4
DR2	12	12	22.5	50	1.84	3.7
DR3	15	10	25	50	1.62	3.2

D. Torque Tracking Tests

We conducted torque tracking experiments during walking and running on a single participant to evaluate the torque control performance under locomotion. The assistive profiles were generated by a high-level controller of which the magnitude, timing, and shape could be adjusted. The profile was constructed by mimicking the human internal joint moment, which is shown in Fig. 11(a) and described in the following:

$$\tau_d(t) = \begin{cases} 2\frac{t}{T_p - T_r}, & 0 \le t < T_p - T_r \\ 2 + (\Gamma_p - 2)\frac{1-\cos\left(\pi \frac{t-T_p+T_r}{T_r}\right)}{2}, & T_p - T_r \le t < T_p \\ \Gamma_p \frac{1+\cos\left(\pi \frac{t-T_p}{T_f}\right)}{2}, & T_p \le t < T_p + T_f \\ 0, & \text{otherwise.} \end{cases}$$

The curve was constructed by two sinusoidal curves and one linear slope, parameterized by four parameters: rise time T_r, fall time T_f, peak time T_p, and peak torque Γ_p. This method of emulating human torques had been used and proved effective in multiple prior publications [1], [2]. We evaluated the torque tracking performance for each actuation configuration under three walking assistance profiles and three running assistance profiles. For either actuation setup in walking or running, its three tested assistance conditions have the same peak torque but different peak time, rising time, and fall time. For the case of single-motor setup, the peak torque values for both assistance profiles of walking and running were 30 N·m. However, the peak time varied from 45% to 50% (SW1–SW3) during walking and from 20% to 25% (SW1–SW3) during running. For the case of dual-motor configuration, the peak torque values of assistance profiles were 60 N·m during walking (DW1–DW3) and 50 N·m during running (DR1–DR3) with the same peak time in a single-motor setup. The profile parameters of the 12 conditions were described in Table II. In each assistance condition, the human subject was asked to walking at 1.25 m·s^{-1} or running at 2.0 m·s^{-1} on a treadmill for 1 min. The measured torque was averaged and the root-mean-squared (rms) tracking errors were calculated over the last 30 steps.

Fig. 11(b) and (c) shows the torque tracking results for single-motor actuation and dual motors configuration during walking and running. Table II also depicts the rms of tracking error in

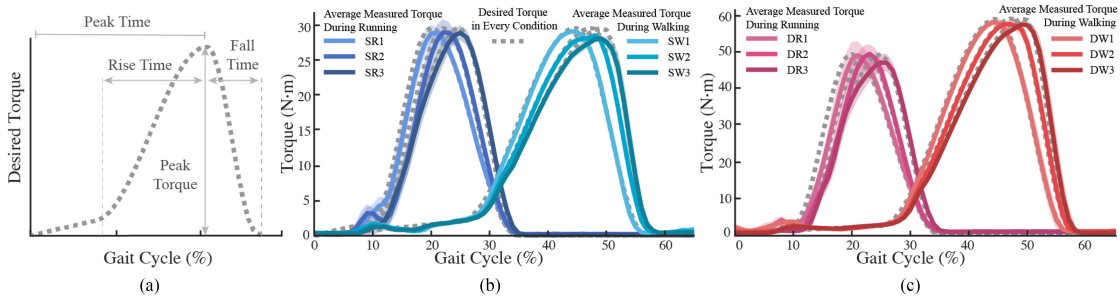

Fig. 11. (a) Parameterized torque profile. Torque tracking results for (b) single- and (c) dual-motor configurations during running and walking under different profiles. In each condition, the human subject was asked to walking at 1.25 m·s^{-1} or running at 2.0 m·s^{-1} on a treadmill. The gray dotted lines show the desired torque of every condition. The solid lines were averaged measured torques. The shadow areas depict the standard deviations.

each profile. The average rms tracking error was 2.5% and 2.7% of peak torque for single- and dual-motor systems, respectively. The average rms tracking error among 12 evaluated profiles was 2.6% of peak torque.

E. Physiological Evaluation

Preliminary physiological experiments were conducted on five healthy participants to evaluate the effectiveness of this mobile ankle exoskeleton under assistance. The participants walked in three conditions: NW condition without wearing the exoskeleton, single-motor-assisted condition, and dual-motor-assisted condition (DW). The rise time, fall time, peak timing, and peak torque of the assistance were 30%, 10%, 48%, and 30 N·m, respectively, for single-motor condition. The timing parameters in dual-motor assisted condition were the same in single-motor condition while the peak torque was set at 50 N·m. The parameters of the assistive torque were set to provide relatively comfortable assistance based on our experience. Note that this article is focusing on system development, and experiments in this section were merely to demonstrate the capabilities of the system, rather than to test its performance capacity or to investigate the human responses. For this reason, we did not include too many participants or optimize human reactions systematically. Soleus muscle activities were measured using surface EMG with wireless electrodes (Trigno, Delsys, USA). The signals were high-pass filtered with a cutoff frequency of 20 Hz, rectified and low-pass filtered with a cutoff frequency of 6 Hz. All results were averaged over the last 30 steps of each condition and normalized by NW condition. Fig. 12 shows the decrease in soleus muscle activity under assistance. Compared with NW, the average decreases in soleus muscle activity among five participants were 24.4 and 32.5% under single-motor assistance and dual-motor assistance, respectively.

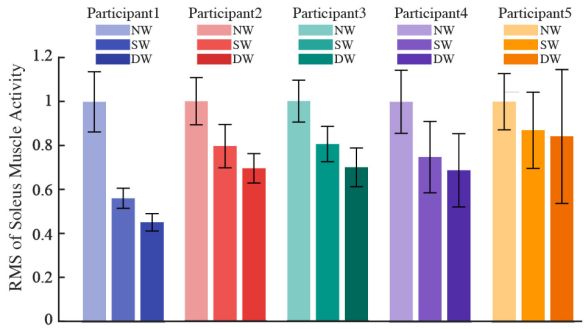

Fig. 12. Evaluation of the exoskeleton's effectiveness in reducing soleus muscle activity. The participants walked in three conditions: normal walking (NW), single-motor actuation assisted (SW) and dual-motor actuation assisted (DW).

IV. Discussion

This article aimed to design a lightweight mobile ankle exoskeleton that can provide a wide range of assistance with accurate torque tracking performance. To balance system weight and actuator power, we utilized modularized actuators to construct a switchable actuation system. The single-motor system can achieve better assistance transparency, which is more suitable for children, the elderly, and patients to improve their mobility. The dual-motor system has high torque capability and can provide more effective assistance in strenuous physical activities, such as load carriage.

Our design has outperformed the existing mobile devices in terms of maximum assistance capacity and torque tracking performance. With 1.7 kg lighter in total mass and 0.45 kg heavier in distal mass, the single-motor system can achieve nearly twice assistive torque compared with Harvard portable ankle exosuit for clinical application [14]. The dual-motor system can provide 142% more assistive torque with only 108% of the weight compared with the MIT autonomous ankle exoskeleton [4]. Both actuation configurations can provide close-loop torque bandwidth higher than 13 Hz under 20 N·m. The real-time torque tracking error is 2.6% of peak torque among 12 evaluated profiles, which is better than reported mobile ankle exoskeletons [4], [14], [15].

The optimized structure of carbon fiber makes the exoskeleton end effector lightweight compliant to wear. The weight of the end effector was reduced to 0.5 kg, which is 40% lighter compared with the previous design [12]. Every carbon-fiber component was designed for special usage. The foot carbon fiber structs were optimized by topology optimization to be high strength, and the thickness of the heel bracket was specially selected to be elastic in the assistive direction.

Modularizing the actuators and connecting them parallelly to achieve higher assistance help ease the design of the mobile

exoskeleton. However, utilizing multimotor will increase the complexity of control. Each motor needs to be calibrated to synchronize. Bandwidth tests and torque tracking tests demonstrated that the proposed torque control algorithm can achieve decent torque tracking performance under dual-motor system. With higher assistance requirements, it can be easily extended by more motors to generate higher assistive torque.

The proposed torque controller was effective for the designed mobile ankle exoskeleton. The current and velocity compensations help the feedback admittance controller to focus on the errors caused by unmodeled dynamics and nonlinearity, which enhances the tracking performance and improves the stability of the controller. During maximum torque tests, bandwidth tests, and torque tracking experiments, the controller shows decent torque tracking performance. The maximum 1.07 N·m of tracking error under 30 N·m peak torque with single-motor actuation and averaged 2.6% rms tracking error among 12 evaluated profiles are outstanding in mobile exoskeletons.

By balancing low distal mass and better control performance, we mounted the actuation on the end effector. In some previous works [2], [5], the actuators were mounted on the waist and the power was transmitted by Bowden cables. This can further decrease distal mass and, thus, lower metabolic penalty, but the bending of Bowden cable will increase the control complexity. Mounting the actuation on the end effector can achieve better control performance. More accurate tracking means less surprises and deviations from the designed behavior, which is crucial for human safety and comfort.

The large decrease in soleus muscles activity demonstrated that both the single- and dual-motor exoskeleton systems have the ability to bring benefits to human body, even without customization or optimization. By utilizing the human-in-the-loop optimization, the mobile ankle exoskeleton is promising to provide more benefits. Results of transparency tests showed that the dual-motor system had comparable transparency with the single-motor one. Compared with the single-motor system, only the maximum ankle dorsiflexion angle shows an obvious decrease of 2.1° under dual-motor actuation. The joint moments at the hip and ankle increase slightly.

Regardless of the advantages of our system, there still exist some issues. The torque tracking performance, even better than most mobile exoskeletons, is inferior to some tethered exoskeleton systems. Limited actuator power and nonlinearity caused by unidirectional cables were the major causes. Control methods based on historical information, such as iterative learning control, can help to overcome that problem. The decreases of ankle joint angle in transparency tests were probably caused by the exoskeleton's additional mass and inertia, which indicated a penalty in metabolic cost. Due to the COVID-19 pandemic, we did not test the metabolic impact of the mobile ankle exoskeleton, which we will investigate in the future.

V. Conclusion

In this article, we present a mobile, lightweight exoskeleton that can provide ankle plantarflexion assistance during locomotion. The exoskeleton comprises a power belt, a lightweight compliant end effector, and a configuration-switchable actuation. The actuation system was designed with modularization that can switch configurations for different individual's needs and various tasks' requirements, helping mobile exoskeletons realize their potential under different scenarios. Admittance control with compensation loops implemented in an integrated real-time embedded system provides high-accuracy torque tracking performance under different assistance profiles and different locomotion conditions. Preliminary biomechanical experiments demonstrated the exoskeleton's transparency and ability of reducing muscles activity. With autonomy, reduced weight, accurate torque tracking, and human response readability, this exoskeleton system can realize human-in-the-loop optimization off the treadmill on the ground. New assistance strategies and optimal assistance patterns on more terrains will lead to more effective gait assistance applications in real life.

References

[1] J. Zhang *et al.*, "Human-in-the-loop optimization of exoskeleton assistance during walking," *Science*, vol. 356, no. 6344, pp. 1280–1284, 2017.
[2] J. Kim *et al.*, "Reducing the metabolic rate of walking and running with a versatile, portable exosuit," *Science*, vol. 365, no. 6454, pp. 668–672, 2019.
[3] C. J. Walsh, K. Endo, and H. Herr, "A quasi-passive leg exoskeleton for load-carrying augmentation," *Int. J. Humanoid Robot.*, vol. 4, no. 03, pp. 487–506, 2007.
[4] L. M. Mooney and H. M. Herr, "Biomechanical walking mechanisms underlying the metabolic reduction caused by an autonomous exoskeleton," *J. neuroengineering Rehabil.*, vol. 13, no. 1, pp. 1–12, 2016.
[5] L. N. Awad *et al.*, "A soft robotic exosuit improves walking in patients after stroke," *Sci. Transl. Med.*, vol. 9, no. 400, 2017.
[6] K. Kong and D. Jeon, "Design and control of an exoskeleton for the elderly and patients," *IEEE/ASME Trans. Mechatronics*, vol. 11, no. 4, pp. 428–432, Aug. 2006.
[7] R. C. Browning, J. R. Modica, R. Kram, and A. Goswami, "The effects of adding mass to the legs on the energetics and biomechanics of walking," *Med. Sci. Sports Exercise*, vol. 39, no. 3, pp. 515–525, 2007.
[8] P. Malcolm, W. Derave, S. Galle, and D. De Clercq, "A simple exoskeleton that assists plantarflexion can reduce the metabolic cost of human walking," *PLoS One*, vol. 8, no. 2, 2013, Art. no. e56137.
[9] S. Galle, P. Malcolm, S. H. Collins, and D. De Clercq, "Reducing the metabolic cost of walking with an ankle exoskeleton: Interaction between actuation timing and power," *J. Neuroengineering Rehabil.*, vol. 14, no. 1, pp. 1–16, 2017.
[10] G. M. Bryan, P. W. Franks, S. C. Klein, R. J. Peuchen, and S. H. Collins, "A hip–knee–ankle exoskeleton emulator for studying gait assistance," *Int. J. Robot. Res.*, vol. 40, no. 4–5, pp. 722–746, 2021.
[11] G. Lee, Y. Ding, I. G. Bujanda, N. Karavas, Y. M. Zhou, and C. J. Walsh, "Improved assistive profile tracking of soft exosuits for walking and jogging with off-board actuation," in *Proc. IEEE/RSJ Int. Conf. Intell. Robots Syst.*, 2017, pp. 1699–1706.
[12] K. A. Witte, J. Zhang, R. W. Jackson, and S. H. Collins, "Design of two lightweight, high-bandwidth torque-controlled ankle exoskeletons," in *Proc. IEEE Int. Conf. Robot. Automat.*, 2015, pp. 1223–1228.
[13] Y. Ding, M. Kim, S. Kuindersma, and C. J. Walsh, "Human-in-the-loop optimization of hip assistance with a soft exosuit during walking," *Sci. Robot.*, vol. 3, no. 15, 2018.
[14] J. Bae *et al.*, "A lightweight and efficient portable soft exosuit for paretic ankle assistance in walking after stroke," in *Proc. IEEE Int. Conf. Robot. Automat.*, 2018, pp. 2820–2827.
[15] Z. F. Lerner *et al.*, "An untethered ankle exoskeleton improves walking economy in a pilot study of individuals with cerebral palsy," *IEEE Trans. Neural Syst. Rehabil. Eng.*, vol. 26, no. 10, pp. 1985–1993, Sep. 2018.
[16] S. L. Delp *et al.*, "Opensim: Open-source software to create and analyze dynamic simulations of movement," *IEEE Trans. Biomed. Eng.*, vol. 54, no. 11, pp. 1940–1950, 2007.